Chapter 29
Signatures of Transient Purely Ballistic Heat Conduction: Theory and Experimental Investigation

Aleksei A. Sokolov, Wolfgang H. Müller, Anton M. Krivtsov, and Alexey V. Porubov

Abstract In this paper, we propose an approach to define thermal conductivity for a purely ballistic transient heat conduction and study its size dependence for two-dimensional structures in circular geometry in order to use this dependence as a purely ballistic regime signature. Then, a review of various experimental techniques by which the thermal conductivity is measured is presented. Finally, the thermal conductivity of graphene in purely diffusive regime is measured for one fixed sample size using Raman thermometry. The result of the proposed theoretical approach is a linear dependence on the sample size in the case of purely ballistic thermal conductivity. An outcome of an experimental study of graphene in a purely diffusive regime and the presented review of experimental methods are the basis for an extension of further experimental studies to the anomalous heat conduction regimes.

Keywords Ballistic heat transport · Ballistic limit · Harmonic crystal · Graphene · Raman · Transient processes · Anomalous heat transport

29.1 Introduction

In recent years, the study of anomalous thermal conductivity, i.e., processes that deviate from the classical Fourier equation, has been actively developing in the scientific community. A number of experimental studies of this anomaly in solid crystals can be found in [10, 11, 26]. A theoretical description of this phenomenon is

A. A. Sokolov (✉) · W. H. Müller
Technische Universität Berlin, Einsteinufer 5, 10587 Berlin, Germany
e-mail: sokolov@tu-berlin.de

W. H. Müller
e-mail: wolfgang.h.mueller@tu-berlin.de

A. M. Krivtsov · A. V. Porubov
Institute for Problems in Mechanical Engineering RAS, V.O., Bolshoy pr., 61, St. Petersburg 199178, Russia
e-mail: akrivtsov@bk.ru

V. A. Polyanskiy and A. K. Belyaev (eds.), *Mechanics and Control of Solids and Structures*, Advanced Structured Materials 164,
https://doi.org/10.1007/978-3-030-93076-9_29

possible by using the kinetic approach (Boltzmann equation), the Maxwell-Cattaneo model [15], the Guyer-Krumhansl model [19], lattice dynamics [20], and some other methods.

The difficulty in connecting the proposed models with processes in real materials lies in the fact that such transient processes occur at very high speeds (speed of sound in crystals, e.g., >10 km/s for graphene [7]). Moreover, since the process is fundamentally different from Fourier's law, it lacks the thermal conductivity coefficient as a material parameter. However, even when Fourier's law does not hold, in an experimental setting and molecular dynamic simulations when a steady non-equilibrium temperature gradient is applied to the specimen, it turns out that it is convenient to use the mathematical formulation of Fourier's law and to observe the size dependence of thermal conductivity as a signature of anomalous regimes [6, 20, 28, 29]. Thus, experimental methods, which have now already become a standard, have been developed to determine the thermal conductivity coefficient from Fourier's law [30]. As an alternative, for example, the thermal grating method deals directly with a non-stationary formulation [11]. However, it has some open questions to consider. For example, the measurement of the thermal process occurs indirectly, through the accompanying thermoelastic process, which, despite the fact that it does not have a significant effect in the classical regime, can become more pronounced in the ballistic regime (see so-called *ballistic resonance* [18]).

In the classical regime of heat conduction, the heat flux is proportional to the gradient of temperature. Accordingly, the coefficient of proportionality (heat conductivity κ) is a material parameter and does not depend on the system size, L. In anomalous heat conduction, the process deviates from the classical Fourier law. A number of theoretical results have shown a power divergence of heat conductivity $\kappa \sim L^{\alpha}$ for 1D systems [20]. This result was confirmed also experimentally [27].

Recently in the laboratory "Discrete Models in Mechanics" IPME RAS under the supervision of A.M. Krivtsov, a ballistic heat conduction model based on the analysis of crystal dynamics was developed [16, 17]. The proposed model has a number of obvious advantages (analytical description, lack of phenomenological assumptions). Despite the fact that there are also some shortcomings (harmonic approximation, lack of quantum effects description) it is undoubtedly promising for the description of ballistic heat propagation from the point of view of continuum mechanics and constitutive theory. For an experimental study of the limits of applicability of this theory and its correspondence to real materials, a joint project with W.H. Müller, Chair of Continuum Mechanics and Constitutive theory of TU Berlin was initiated. The group has extensive experience in experimental work on a micro-level and expertise in continuum mechanics [1, 21, 22].

In order to connect the two descriptions, non-stationary ballistic model and the classical Fourier thermal conductivity coefficient, a theoretical method is proposed in this work, based on a definition of thermal conductivity for transient ballistic processes originally suggested in [17]. Furthermore, experimental studies using the methods available in the laboratory of TU Berlin and a review of works on this topic are presented. Last, an experimental measurement of the thermal conductivity of graphene is performed. Graphene was chosen as the material of investigation

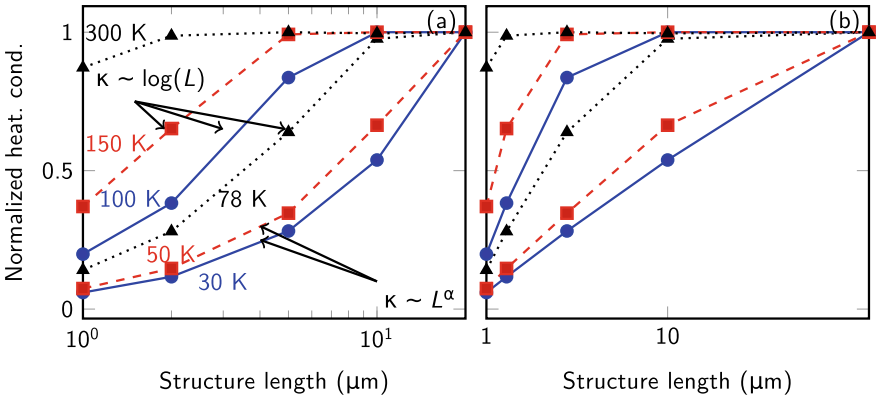

Fig. 29.1 Dependence of thermal conductivity on length of the structure at different temperatures, **a** logarithmic scale, **b** linear scale. The data for each curve is normalized to its value at $L = 20\,\mu\text{m}$. Graphs are plotted using data from [29]

because, first, it has great potential for technological applications in microelectronic devices. Second, its greatest importance is that it is cheap to manufacture and it is possible to produce ultrapure defect-free monocrystalline samples (grain size up to $20\,\mu\text{m}$). Thus, graphene appears to be a very convenient playground for experimental verification of the abovementioned theoretical predictions.

Theoretical results presented in [20] for 2D anharmonic systems show a logarithmic divergence of thermal conductivity $\kappa \sim \log(L)$. This is confirmed by experimental results with graphene for a quadrilateral over a large temperature range [32] and for circular geometries at room temperature (RT) [8, 12], and also by numerical simulation at RT for circular geometry [4]. Numerical simulations of 2D FPU systems[1] in [31] showed a logarithmic divergence for $\alpha\beta$-FPU and purely quartic models, and a power divergence for β-FPU systems. In [29], a kinetic theory was used and third-order terms in the Hamiltonian were taken into account. The results [29] indicate a logarithmic divergence for temperatures approximately above liquid nitrogen temperatures and a power divergence below (see Fig. 29.1). These findings for 2D materials showing power divergence are of special interest, since at very low temperatures the influence of anharmonicity decreases and a purely ballistic heat conduction regime is achievable.

The rest of this paper is structured as follows. In Sect. 29.2, thermal conductivity is defined for the equations of ballistic heat conduction and its size dependence is investigated. In Sect. 29.3, a review of experimental techniques and results of measurements performed at TU Berlin are presented. The size dependence of thermal conductivity obtained theoretically from ballistic model in previous section is compared with available experimental data. Section 29.4 closes with a conclusion.

[1] FPU = Fermi-Pasta-Ulam.

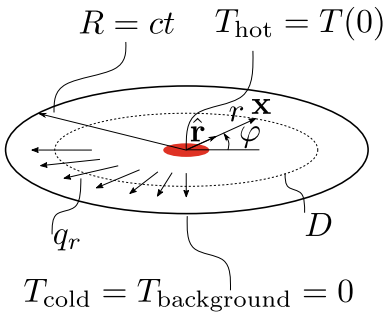

Fig. 29.2 Schematic representation of the considered anomalous heat conduction process

29.2 Divergence of Heat Conductivity for Transient Purely Ballistic Heat Conduction

An engineering approach to the definition of thermal conductivity stems from the problem of two regions with temperatures T_{hot} and T_{cold}, separated at a distance L with a medium with thermal conductivity κ. In a classical diffusive heat conduction regime, a linear temperature profile results with uniform heat flux q. In this case, heat conductivity is defined as

$$\kappa = \frac{qL}{\Delta T}, \quad \Delta T = T_{\text{hot}} - T_{\text{cold}}. \tag{29.1}$$

When studying anomalous heat conduction, the heat flux is not uniform. This was observed, for example, in one-dimensional discrete systems [20]. For a one-dimensional system of N particles between hot and cold reservoirs separated by a length L, an averaged heat flux is defined as $\langle q \rangle = \sum_n q_n / N$, where q_n is a local per particle heat flux and a definition for the thermal conductivity similar to (29.1) results, $\kappa = \langle q \rangle L / \Delta T$. The same approach is possible for bulk systems [28] where a spatial average over the volume between the reservoirs is used.

Let us consider the anomalous heat flux in two-dimensional materials. It was shown in [16] that a fundamental solution for the kinetic temperature field for a purely ballistic heat conduction regime is a self-similar function, which can be represented as

$$T = \frac{1}{t^2} f\left(\frac{r}{t}\sin\varphi, \frac{r}{t}\cos\varphi\right), \quad r < R, \tag{29.2}$$

where r, φ are polar (radial and angular, respectively) coordinates, $R = ct$, and c is the fastest group velocity in the system. For $r > R$, the temperature field remains zero (we assume a background temperature of zero).

The process described by this fundamental solution has the following features. Initially, a point perturbation is applied at the point of origin. Then the heat flows from the center radially away forming a growing circle with a radius increasing at a constant speed. Outside of this circle the temperature remains zero, see Fig. 29.2.

Applying the approach subsumed in formula (29.1), the thermal conductivity can be defined as follows. Heuristically we fix the moment of observation time and restrict the considered space to the circle inside which by the moment of observation the energy has spread radially. Then the average heat flux, which is to be substituted in (29.1) and which causes the energy spread from the heated center to the colder boundary, is the average of a radial component of flux over the whole area of this circle,

$$\langle q \rangle = \frac{\int\limits_S \mathbf{q} \cdot \hat{\mathbf{r}} \, \mathrm{d}S}{S} = \frac{\int\limits_0^{2\pi} \int\limits_0^R q_r(r, \varphi) r \, \mathrm{d}r \, \mathrm{d}\varphi}{\pi R^2}, \tag{29.3}$$

where $\hat{\mathbf{r}}$ is the radial vector and S is the area of the circle.

The temperature difference in the denominator of (29.1) between hotter and colder regions will be in this axisymmetric case given by the difference between the temperature in the center, from which the heat flows radially away, and the temperature of the background toward which the heat flows. Since the background temperature is zero the temperature difference is $\Delta T = T(0)$.

As an approximation, we assume that the temperature profile can be factorized into radial and angular components,

$$T(r, \varphi) = \frac{1}{t^2} f\left(\frac{r}{t} \sin\varphi, \frac{r}{t} \cos\varphi\right) \approx \frac{1}{t^2} \Theta\left(\frac{r}{t}\right) \Phi(\varphi) . \tag{29.4}$$

Although this may be not strictly true, the author believes that the main factor which contributes to the thermal conductivity within this framework is the flux in the direction of the radial component along which the heat transfers from the hotter (center) to the colder (boundary) region. The heat flux is also factorized as

$$q_r \approx \hat{q}_r(r, t) \, \Psi(\varphi) . \tag{29.5}$$

A more precise form of heat flux function will be presented later.

Substituting the averaged heat flux (29.3) into the thermal conductivity (29.1) and taking for the length of the system the radius of the circle, $L = R$, yield

$$\kappa = \frac{\langle q \rangle R}{\Delta T} = \int\limits_0^{2\pi} \Psi(\varphi) \, \mathrm{d}\varphi \frac{\int\limits_0^R \hat{q}_r(r, t) r \, \mathrm{d}r}{\pi R T(0)} . \tag{29.6}$$

We are interested in the proportionality dependence of the thermal conductivity but not in its absolute value. Therefore, by recalling $R = ct$ and by omitting the constant arising from integration of angular component and other constants, one obtains the following proportionality:

$$\kappa \sim \frac{\int\limits_0^R \hat{q}_r(r,t) r \, \mathrm{d}r}{tT(0)} \sim t \int\limits_0^R \hat{q}_r(r,t) r \, \mathrm{d}r, \tag{29.7}$$

where the last proportionality arises, because it can be seen from (29.2) that $T(0) \sim 1/t^2$.

Let us consider the local energy balance equation,

$$\rho \dot{u} = -\nabla \cdot \mathbf{q}, \tag{29.8}$$

and integrate it over the surface of a circle $D : |\mathbf{x}| \leq r$,

$$\int\limits_{S \in D} \rho \dot{u} \, \mathrm{d}S = - \int\limits_{S \in D} \nabla \cdot \mathbf{q} \, \mathrm{d}S. \tag{29.9}$$

According to divergence theorem, the right-hand side of this equation transforms into

$$\begin{aligned} \int\limits_{S \in D} \nabla \cdot \mathbf{q} \, \mathrm{d}S = \int\limits_{l \in \partial D} \mathbf{q} \cdot \mathbf{n} \, \mathrm{d}l = \int\limits_0^{2\pi} \hat{q}_r(r,t) \Psi(\varphi) r \, \mathrm{d}\varphi = r \hat{q}_r(r,t) \int\limits_0^{2\pi} \Psi(\varphi) \, \mathrm{d}\varphi \\ = C_1 r \hat{q}_r(r,t), \end{aligned} \tag{29.10}$$

where ∂D is the circle boundary, normal to which is a radial unit vector $\mathbf{n} = \hat{\mathbf{r}}$, $\mathrm{d}l = r \, \mathrm{d}\varphi$. C_1 is the constant arising from integration of the angular part of heat flux. The left-hand side together with $u = c_V T$, where c_V is the specific heat capacity at constant volume, gives

$$\begin{aligned} \int\limits_{S \in D} \rho \dot{u} \, \mathrm{d}S = \rho c_V \int\limits_{S \in D} \dot{T} \, \mathrm{d}S = \int\limits_0^{2\pi} \Phi(\varphi) \, \mathrm{d}\varphi \int\limits_0^r \frac{\partial}{\partial t} \left[\frac{1}{t^2} \Theta\left(\frac{\tilde{r}}{t} \right) \right] \tilde{r} \, \mathrm{d}\tilde{r} = \\ = C_2 \int\limits_0^r \frac{\partial}{\partial t} \left[\frac{1}{t^2} \Theta\left(\frac{\tilde{r}}{t} \right) \right] \tilde{r} \, \mathrm{d}\tilde{r}. \end{aligned} \tag{29.11}$$

Expanding time derivative in the last equality yields

$$\frac{\partial}{\partial t} \left[\frac{1}{t^2} \Theta\left(\frac{\tilde{r}}{t} \right) \right] = -\frac{2}{t^3} \Theta\left(\frac{\tilde{r}}{t} \right) - \frac{\tilde{r}}{t^4} \Theta'\left(\frac{\tilde{r}}{t} \right), \tag{29.12}$$

where the dash $(\ldots)'$ denotes differentiation with respect to the argument. Substituting it back to (29.11) leads to

$$\int\limits_{S\in D} \rho\dot{u}\,\mathrm{d}S = -\frac{C_2}{t}\int_0^{r/t}\left[2\Theta\left(\frac{\tilde{r}}{t}\right)+\frac{\tilde{r}}{t}\Theta\left(\frac{\tilde{r}}{t}\right)\right]\frac{\tilde{r}}{t}\,\mathrm{d}\frac{\tilde{r}}{t} = -\frac{C_2}{t}\zeta\left(\frac{r}{t}\right). \quad (29.13)$$

A combination of (29.10) and (29.13) yields an expression for the radial component of the heat flux,

$$\hat{q}_r(r,t) = \frac{C_3}{rt}\zeta\left(\frac{r}{t}\right), \quad C_3 = C_2/C_1. \quad (29.14)$$

Substitution of (29.14) into the integral in (29.7) gives

$$\int_0^R \hat{q}_r(r,t)r\,\mathrm{d}r = \int_0^{ct}\frac{C_3}{t}\zeta\left(\frac{r}{t}\right)\mathrm{d}r = \int_0^c C_3\zeta\left(\frac{r}{t}\right)\mathrm{d}\frac{r}{t} = \text{const}. \quad (29.15)$$

Thus, from (29.15) and (29.7) it follows that

$$\kappa \sim t. \quad (29.16)$$

It is also seen from (29.15) that the average heat flux in this process is constant, $\langle q\rangle = \text{const}$. Therefore, proportionality of thermal conductivity is determined by the ratio $R/T(0)$. Recalling that $R = ct$, and $T(0) \sim 1/t^2$ this result is directly obtained.

By using the result (29.16) and $t = R/c$ it also follows that

$$\kappa \sim R. \quad (29.17)$$

Formula (29.17) shows that the thermal conductivity diverges linearly with the disk radius R. Note that mostly in anharmonic systems the dependence is not of the power type but logarithmic. One of the publications [31] shows a power (but not a linear) dependence for β-FPU system.

29.3 Experimental Techniques

A conventional experimental technique for measuring a coefficient of heat conductivity κ is to apply a temperature difference on the boundaries of the system and to measure a steady heat flux. Heat conductivity is then calculated from Fourier's law. For a circular symmetry, the heating is usually applied to the center of the system under observation so that a temperature difference is established between the center and the boundary of the examined disk. We consider the following mathematical formulation of the problem. A graphene disk with radius R is heated in the center by a laser. The boundary is held at ambient temperature. The heat production $q(r)$ is assumed to be Gaussian within the plane:

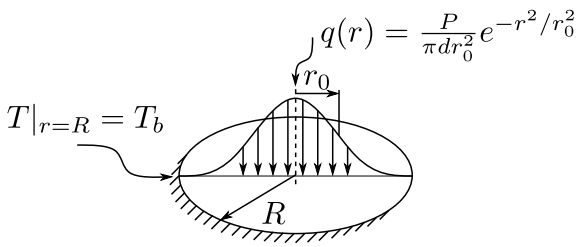

Fig. 29.3 Heat production of the Gaussian type in a circular membrane

$$q(r) = \frac{P}{\pi d r_0^2} e^{\frac{r^2}{r_0^2}}, \tag{29.18}$$

where d is the thickness of graphene, r_0 is the theoretical Gaussian spot size.

The situation is presented in Fig. 29.3. In order to describe a steady temperature profile, let us consider the diffusive Fourier equation in cylindrical coordinates with a production term $q(r)$:

$$\kappa \frac{1}{r} \frac{\mathrm{d}}{\mathrm{d}r} \left(r \frac{\mathrm{d}T}{\mathrm{d}r} \right) + q(r) = 0. \tag{29.19}$$

We introduce the dimensionless variable $\tilde{r} = r/r_0$. By integrating Eq. (29.19), we get the solution as follows:

$$\begin{aligned} T(\tilde{r}) - T(0) &= \frac{1}{2} \frac{P}{\pi d \kappa} \int_0^{\tilde{r}} \frac{1 - e^{-x^2}}{\mathrm{x}} dx = \\ \frac{1}{2} \frac{P}{\pi d \kappa} &\left(\ln \tilde{r} - \frac{1}{2} \mathrm{Ei}(-\tilde{r}^2) + \frac{\gamma}{2} \right) \approx \frac{1}{2} \frac{P}{\pi d \kappa} \left(\ln \tilde{r} + \frac{\gamma}{2} \right), \end{aligned} \tag{29.20}$$

where Ei is the exponential integral function, γ is the Euler's constant. Then if the drop of the temperature between temperature in the center T_c and the boundary T_b is known one can express the heat conductivity by the formula:

$$\kappa = \frac{1}{2} \frac{P}{\pi d \left(T_c - T_b \right)} \left(\ln \frac{R}{r_0} + \frac{\gamma}{2} \right). \tag{29.21}$$

29.3.1 Raman Thermometry

Introductory Remarks

Raman thermometry was introduced in the work of Balandin and colleagues [3, 5]. The laser beam is used as a heating source in the center of a membrane and at the same time as a probe. In order to apply this technique successfully, the graphene membrane must be attached to an efficient heat sink. The temperature of a boundary can then be assumed to have ambient temperature. By knowing the laser power and a

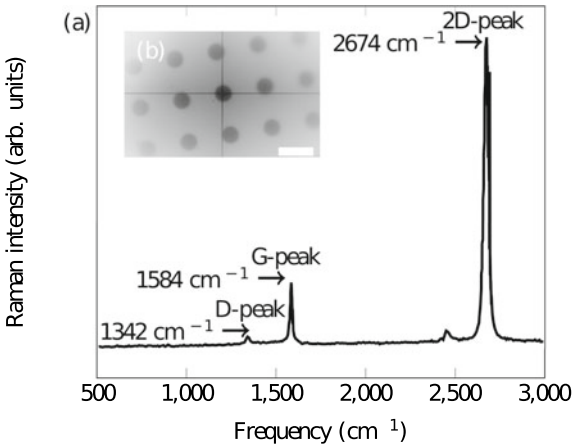

Fig. 29.4 **a** Room-temperature Raman spectrum from single-layer suspended graphene **b** optical microscope image of the sample. The scale bar is 5 μm

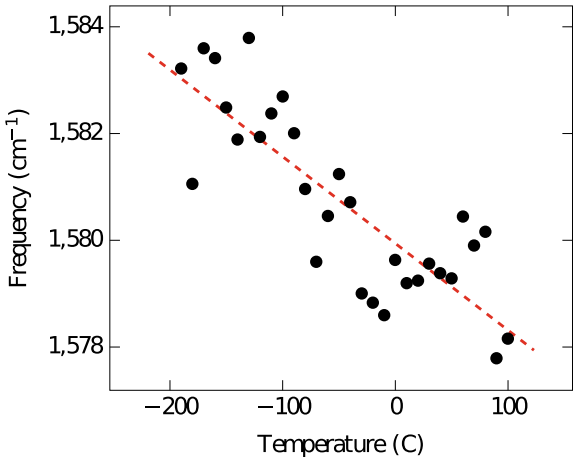

Fig. 29.5 Temperature dependence of G-peak position of a single-layer graphene (black dots) and linear fit (red dashed line). The graph is plotted using data from [3]

coefficient of absorption, and by combining it with measured temperature difference the coefficient of heat conductivity is calculated by using formula (29.21).

The spectrum of a suspended single-layer graphene at room temperature is presented in Fig. 29.4. Characteristic features are the G-peak located around ca. 1580 cm^{-1} and the D-peak located around ca. 1380 cm^{-1}. It was observed in [3] that an increase of temperature leads to a red shift of the G-peak. The dependence of the G-peak position on the temperature of a graphene on a substrate is presented in Fig. 29.5 (data taken from [3]).

The temperature dependence of a G mode can be described by the following equation (after [3]):

$$\omega = \omega_0 + \chi T, \tag{29.22}$$

Table 29.1 Temperature coefficient of single-layer graphene

Substrate	χ (cm^{-1}/K)	Method	Comment	Ref.
SiO_2	−0.015	External heating	–	[3]
SiO_2	−0.03	External heating	–	[25]
Suspended	−0.0405	External heating	–	[2]
–	−0.03	MD	AIREBO, quasilinear	[14]
–	−0.06	MD	LCBOP, quasilinear	[14]
–	−0.0517	MD	Tersoff-2010	[14]

Table 29.2 Coefficient of optical absorption of single-layer graphene

Optical absorption coefficient α	Wavelength nm	Ref.
$3.4 \pm 0.7\%$	532	[2]
$2.3 \pm 0.1\%$	500–740	[24]
$2.3 \pm 0.2\%$	1033–2479	[23]
$2.9 \pm 0.2\%$	532	[5]

where ω_0 is the frequency of the G mode when the temperature is extrapolated to 0 K, χ is the temperature coefficient, calculated from a slope of linear fit.

Temperature coefficients calculated in a number of publications are presented in Table 29.1. In numerical calculations [14], several interatomic potentials were considered. Only the Tersoff-2010 potential was able to reproduce the linear G-peak shift observed in the experiments, while LCBOP and AIREBO potentials show a nonlinear, non-monotonic behavior at low temperatures, which deviates from the experimental results. At higher temperatures, these two potentials show a quasilinear behavior with temperature coefficients presented in Table 29.1.

By applying this technique one can use the reflected laser light as a thermometer and determine the temperature difference in (29.21). When knowing the coefficient of optical absorption of graphene α and the power of incident laser P_I the absorbed power P is calculated $P = \alpha P_I$. Then κ is calculated from (29.21). The coefficients of optical absorption obtained in recent publications are presented in Table 29.2. A conventional method to measure the absorption is to measure the difference between the laser power with a power meter, first through an empty hole and then through a suspended graphene membrane [2, 5].

Coefficients of thermal conductivity from various references are presented in Table 29.6. The disadvantage of this method is that the spatial resolution is limited by the diffraction limit $\sim 1\,\mu$m. Therefore, systems bigger than $1\,\mu$m do not allow to investigate ballistic transport at RT with this method since ballistic transport is observed at RT only at smaller scales. Thus, in Table 29.6, the values of heat con-

Table 29.3 Laser power in % of maximum power of source and absorbed power

% Max power	0.1	0.5	1	5	10	50
Incident power mW	39e-3	196e-3	0.36	2.69	4.91	27.46
Absorbed power mW	9e-4	4.5e-3	0.008	0.06	0.11	0.63

duction that correspond to a diffusive regime when κ is a material parameter are presented.

We assume temperature coefficient for G-peak to be equal $\chi = -0.04\,\mathrm{cm}^{-1}/\mathrm{K}$ [2] and an optical absorption of graphene 2.3% [24]. The power of laser can be changed with the steps of ..., 0.1%, 0.5%, 1%, 5%, 10%, 50%, 100% of the maximum working power. It gives us the following correspondence with absorbed laser power complied in Table 29.3.

The beam power was measured by using an Edmund Optics Touchscreen Laser Power Meter with beam spread on the aperture of the sensor with a 5x magnification objective. We performed the experiments with different powers of laser excitation in order to obtain the G-peak shift as a function of absorbed laser power. By using the temperature coefficient and the relations (29.22) the corresponding temperature difference is calculated. The powers 0.1%, 0.5%, 1% do not cause any noticeable peak shift and correspond to the ambient temperature peak position. The power of 50% was excluded from the investigation because it was visually seen that illumination of the substrate occurred at this power, which could cause additional power generation at the boundary. Thus, the peak shift is calculated as difference of peak positions at powers 0.5% and 10%. $\Delta\omega = \omega_{0.5\%} - \omega_{10\%}$.

Materials and Measurement

In the experiment, TEM grids made of gold are used as a support for the substrate. The Au grid is 300 mesh with size between the bars 63 μm. The grid is covered with the amorphous carbon film. The thickness of the carbon film is about 12 nm and it has 2 micron holes, see Fig. 29.4b. Monoatomic graphene layer grown by chemical vapor deposition is transferred over carbon layer (covering the holes), $d = 305\,\mathrm{nm}$. For Raman measurements $\lambda = 532\,\mathrm{nm}$ laser source with a 100x objective and numerical aperture NA = 0.85 is used, which gives theoretical Gaussian spot size used in Eq. (29.18) $r_0 = \lambda/\pi\mathrm{NA} = 0.19\,\mu\mathrm{m}$.

In order to ensure reproducibility, we performed ten measurements of a peak shift $\Delta\omega$ with ten different graphene disks, where the presence of graphene was confirmed by obtaining the Raman spectrum of graphene. The measurements were conducted as follows. First the Raman G-peak was measured by acquisition at 0.5% for 120 s. Then spectral acquisition was done at 10% power for 120 s. This time length of spectral acquisition was chosen in order to ensure a steady state to be established in the graphene sheet, and to acquire enough intensity at low power.

Table 29.4 Peak positions at 0.5% and 10% incident beam powers and frequency shift $\Delta\omega$ (cm $^{-1}$) measured at ten different membranes

No.	$\omega_{0.5\%}$	$\omega_{10\%}$	$\Delta\omega$
1	1583.55	1580.95	2.6
2	1581.82	1578.94	2.88
3	1587.35	1584.25	3.1
4	1585.15	1581.89	3.26
5	1586.38	1582.24	4.14
6	1584.17	1580.84	3.33
7	1583.55	1580.35	3.2
8	1584.56	1581.9	2.66
9	1585.57	1581.96	3.61
10	1584.81	1581.26	3.55

Table 29.5 Heat conductivity κ at 10% incident beam power measured for ten different membranes

No.	κ (W/mK)	No.	κ (W/mK)
1	2292	6	2069
2	1922	7	1828
3	1439	8	1789
4	1862	9	2240
5	1651	10	1678

Table 29.6 RT heat conductivity of graphene measured using Raman thermometry and comparison with the theoretical works

κ (W/mK)	Comment	Ref
4419	0.01% ^{13}C	[5]
2792	1.1% ^{13}C	[5]
2197	50% ^{13}C	[5]
2826	99.2% ^{13}C	[5]
600	–	[9]
1877	–	This work
2622	Kinetic theory	[29]
1910	Theory, in plane graphite	[13]

The measured peak shift and the heat conductivity are presented in Tables 29.4 and 29.5, respectively. The obtained values lead to a mean value of 1877 W/mK with standard error $\sigma^{\text{std}}/\sqrt{N} = 252$ W/mK, where σ^{std^2} is the dispersion and $N = 10$ is the number of measurements.

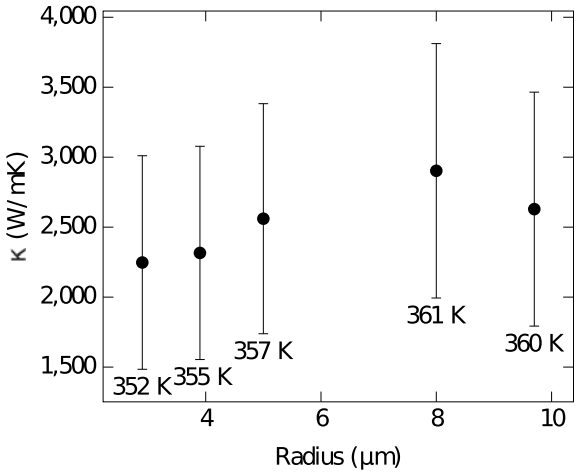

Fig. 29.6 Dependence of heat conduction coefficient of size of graphene disks at near-RT's. The graph is plotted using data from [2]

From [2] (see Fig. 29.6), it is difficult to say anything about size dependence of heat conductivity at room temperature due to the large error. It is concluded [2] that the effect of size dependence is not observed due to high uncertainty, defects, and other impurities of membranes.

29.3.2 Scanning Thermal Microscopy

Another technique to study heat conduction in materials is Scanning Thermal Microscopy (SThM), which is based on Atomic Force Microscopy (AFM). The temperature scan is achieved by measuring the changing resistance in a wire running through an AFM probe. A conventional design of the device is given as follows. A wire made of material with known thermal coefficient (e.g., platinum) is passed thorough the AFM cantilever tip and acts as a nano-thermometer (see Fig. 29.7c, d). The device consists of voltage source (1.), variable resistor (2.) with electrical resistance $\mathcal{R}$, platinum sensor (3.) with electrical resistance $\wp$, digital voltmeter, which is read by a computer software, and the ammeter (5.) (see Fig. 29.7a) the output of which can be seen at the digital readout on the thermoresistor signal amplifier, Fig. 29.7b. Photos, Fig. 29.7b, c, were taken in TU Berlin, Chair of Continuum Mechanics and Constitutive Theory.

Let us consider the working principle in more detail. The goal is to measure the resistance of the platinum wire $\wp$. A voltage source provides a constant voltage U_{in}. By using the knob (2.) the resistance $\mathcal{R}$ in the circuit can be changed. Then the current in the system is calculated using the following formula:

$$I = \frac{U_{\text{in}}}{\wp + \mathcal{R}}. \tag{29.23}$$

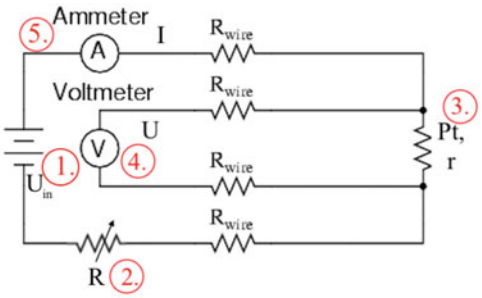

(a) Electrical scheme of thermoresistive measurement circuits.

(b) Photo of thermoresistor signal amplifier

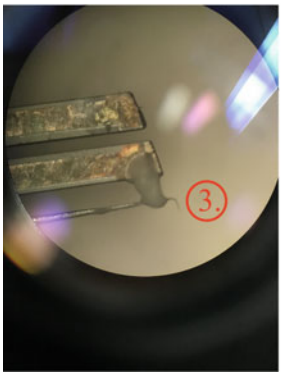

(c) Optical microscope photo of Thermoresistive MV 2000 ™AFM tip on a tuning fork.

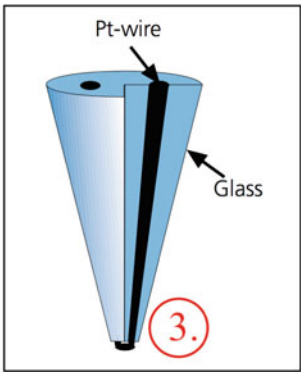

(d) Sketch of Dual-Wire Thermoresistive Probe with fused junction whose resistance is temperature-dependent.

Fig. 29.7 Thermoresistor measurement system layout

If $\mathcal{R} >> \text{»}$ the changes of thermometer resistance » (3.) do not affect the current I significantly. Thus by changing $\mathcal{R}$ it is possible to control the value of the current. The voltage source (1.) and the resistance (2.) connected in series can be considered as a constant current source if the auxiliary resistance connected to the system is relatively small compared to $\mathcal{R}$. Thus the current in the system can be calculated using the following relation and the ammeter (5.):

$$I \sim \frac{U_{\text{in}}}{\mathcal{R}}. \tag{29.24}$$

The desired resistance » at the tip (3.) is defined by the voltage drop measured by the digital voltmeter (4.) The advantage of the scheme is that any voltage dropped across the main current-carrying wires will not be measured by the voltmeter, and so do not enter into the resistance calculation at all. The sought resistance is then measured as follows:

$$\mathcal{R} = \frac{\text{Voltmeter indication}}{\text{Ammeter indication}}. \tag{29.25}$$

One can set the current constant and monitored directly from ammeter, and map only the change of the voltage as a function of position of cantilever (x, y). Let us indicate the voltmeter indication by $U(x, y)$ and the ammeter indication simply by I. Then the electrical resistance map across the surface is $\mathcal{R}(x, y) = U(x, y)/I$. However, one is interested in the temperature map. The temperature of the tip can be found by using the formula

$$\mathcal{R} = \mathcal{R}_0(1 + \alpha T), \qquad T(x, y) = \frac{\text{»}(x, y)/\mathcal{R}_0 - 1}{\alpha} = \frac{U(x, y)/I\mathcal{R}_0 - 1}{\alpha}, \tag{29.26}$$

where $\mathcal{R}_0$ is the resistance at 0 C°, and $\alpha = 0.0038\,\text{C}^{-1}$ is the thermal coefficient of Platinum.

If the applied current is low and does not cause Joule heating the device is operating in a passive mode and if tip and the surface are in thermal equilibrium the temperature of the surface is measured.

If the applied current is higher the device acts as a heat source and the heat is absorbed by the surface. Such a regime is called active. By knowing the supplied power, the theoretical model of absorption, and the read temperature of the tip, one can calculate coefficient of heat conductivity. This measurement is based on the equation

$$R^{\text{th}}\dot{Q} = \Delta T = T_{\text{p}} - T_{\text{amb}}, \tag{29.27}$$

where $R^{\text{th}}[K/W]$ is thermal resistivity, ΔT is the temperature difference between the point of power generation T_{p} and the heat sink, and $\dot{Q}$ is the heat transfer rate or the power of heat generation. Conventionally, it is the difference between temperature of the tip, which is measured from (29.26) and the substrate, which is held at ambient temperature T_{amb}. Two techniques are used to measure R^{th}: (a) a feedback loop is used to keep T_{p} constant by applying different heating power $\dot{Q}$, and then the resistance is

inversely proportional to measured power $R^{\text{th}} = \text{const}/\Delta T$ and (b) using a constant heating power and measure temperature T_{p} of the probe, and then the resistance is proportional to the measured temperature difference $R^{\text{th}} = \text{const}\ \Delta T$.

The power of heat generation $\dot{Q}$ is caused by Joule's heating of the tip and can be calculated directly from measurements $\dot{Q} = IU$:

$$\dot{Q} = \text{Voltmeter indication} \times \text{Ammeter indication}. \tag{29.28}$$

The measured thermal resistance usually combines contributions from several elements. For example [8], it can be

$$R^{\text{th}} = R_{\text{t}} + R_{\text{c}} + R_{\text{spr}}, \tag{29.29}$$

where R_{t} is thermal resistance of probe tip, R_{c} is the contact resistance between tip and sample, and R_{spr} is the thermal spreading resistance into the specimen. We are usually interested in R_{spr}. Difficulties can occur during the determination of R_{c} and R_{t} when the heat conduction is anomalous. The advantage of this technique is a high spatial resolution (up to 17 nm as reported in [8], 20 nm in [12]).

A correlation between thermal resistance and heat conductivity in central symmetry can be obtained from the solution of the heat conduction problem in cylindrical coordinates as a function of radial coordinate r. A thick-walled cylinder is held at temperature T_{c} at the inner surface, $T|_{r=r_0}$ with a heat flux q, $\partial T/\partial r = -q/\kappa$. The solution of a homogeneous Laplace equation in cylindrical coordinates

$$\frac{1}{r}\frac{\partial}{\partial r}\left(r\frac{\partial T}{\partial r}\right) = 0 \tag{29.30}$$

is

$$T(r) = -\frac{qr_0}{\kappa}\ln\frac{r}{r_0} + T_{\text{c}}. \tag{29.31}$$

Let us denote the temperature of the outer boundary $r = R$ by T_b, $\Delta T = T_c - T_b$. Then from (29.31) the following relation holds:

$$q = \frac{\kappa}{r_0 \ln(R/r_0)}\Delta T. \tag{29.32}$$

The heat transfer rate is then calculated as the product of the heat flux and the area of inner surface $S = 2\pi r_0 d$. This leads to

$$\dot{Q} = \frac{2\pi d\kappa}{\ln R/r_0}\Delta T = \frac{1}{R^{\text{th}}}\Delta T \quad \Rightarrow \quad \kappa = \frac{\ln R/r_0}{2\pi d R^{\text{th}}}. \tag{29.33}$$

In [8, 12], SThM was applied to measure heat conduction phenomena on a submicron scale, see Figs. 29.8 and 29.9. The presence of ballistic heat conduction was observed in both references. Both show a logarithmic trend of heat conduc-

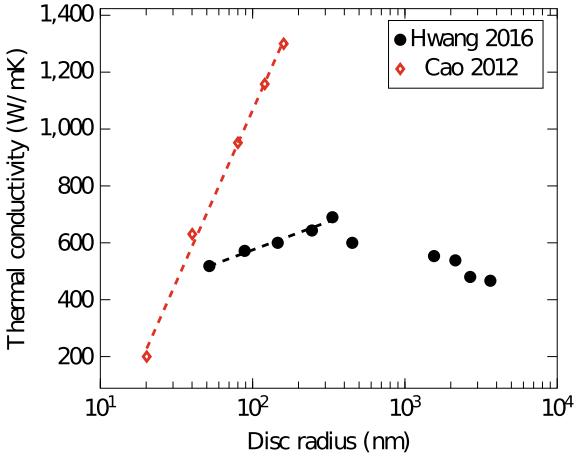

Fig. 29.8 Dependence of thermal conductivity on radius of graphene disk at RT. Graphs are plotted using data from [4, 12]. Dashed lines were added for convenience

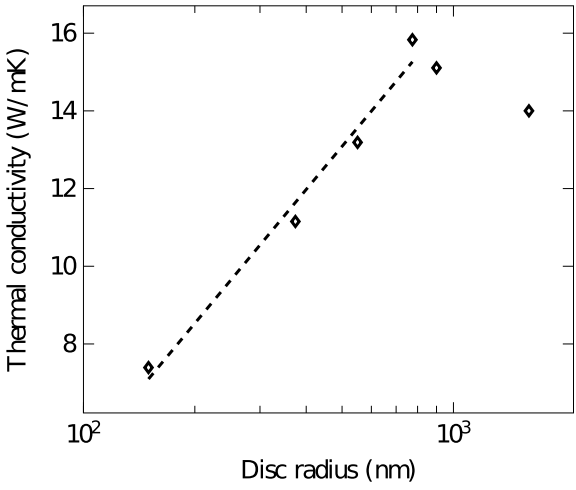

Fig. 29.9 Dependence of thermal conductivity graphene disk + probe tip at RT. Values are calculated with Eq. 29.33 with thermal resistances taken from [8]. A dashed line was added for convenience

tion divergence on scales $<\sim$ 800 nm. In both papers, an interesting decrease of heat conductivity was observed at larger scales. This effect may be attributed to the very small size of the heat source. Figure 29.9 shows the values of heat conduction obtained by Eq. (29.33) with thermal resistances including all contributions as shown in Eq. (29.29) taken from [8]. It was shown in [8] that the thermal resistance of the substrate is several magnitudes lower than the measured full resistance. Thus it can be neglected. It was shown that the value of the tip-sample contact remains constant. Thus it does not influence the size dependence. Yet no absolute values were given. This explains the extremely low values obtained of heat conduction (with respect to what presented in literature for graphene) in Fig. 29.9, since it reflects the conduction of graphene membrane + tip-sample contact. The absolute values reported by [12] are about 600 W/mK, which is relatively low when compared to most results obtained

with optothermal techniques, but it corresponds to the result in [9]. A numerical study [4] confirms the logarithmic trend observed in experimental investigations [8, 12] but does not represent non-monotonic behavior since only systems smaller than 800 nm were studied. Absolute values of thermal conductivity [4] (∼300 W/mK the largest value corresponding to largest investigated sample size) are larger than reported in [8, 12] and closer to values predicted by theory [13] and optothermal technique (see Table 29.6).

29.4 Conclusions

A scientific group from the Technical University of Berlin assessed the possibility of experimental measurement of the thermal conductivity in the case of anomalous heat transfer corresponding to the theoretical estimates of scientists from the laboratory "Discrete Models of Mechanics" IPME RAS within the framework of the international cooperation RSF-DFG. A theoretical approach which allows to define thermal conductivity in transient ballistic case and compares it with steady state measurements was proposed. The results showed that the heat conductivity is power dependent on size (in this particular case, the dependence is linear), such that $\kappa \sim R$, Eq. 29.17. This contradicts to a logarithmic dependence reported in a number of experimental and theoretical studies for anomalous heat transport. On the other hand, some studies [29, 31] also predict a power dependence of heat conductivity in 2D structures at very low temperatures and spatial scales. This raises the question as to whether a logarithmic dependence corresponds to ballistic or some intermediate (between ballistic and diffusive) quasi-ballistic regime of heat conduction. This, in principle, gives rise to further theoretical and experimental challenges.

Experimental techniques that can be used for investigation of the size dependence were also considered in this paper. Raman thermometry is a promising candidate for such studies. However, the effect of power size dependence or any size dependence was not yet observed in the reviewed literature. The difficulty lies in the relatively large minimum size of the laser spot limited by optical diffraction, which is comparable to the phonon mean free path in graphene at RT and in the low-temperature resolution, which causes high uncertainty. A value of ∼1900 W/mK was obtained by using this method in the current work.

Scanning thermal microscopy is another suitable method. Its main advantage is high spatial and temperature resolution. Complications arise in determining additional thermal resistances contributions, along with the sought thermal resistance of the specimen, to the measured value. By using this technique a logarithmic dependence of the heat conduction coefficient on size was observed at the sub-micron scale.

The goal of further research is to measure the size dependence of heat conduction in circular graphene disks using the aforementioned methods and to compare it with the theoretical predictions presented in the current work.

Acknowledgements The proposed theoretical and experimental approaches lay the foundation for further studies of ballistic heat propagation in crystals within the framework of projects of the German Research Foundation (DFG) (Grant No. 405631704) and the Russian Science Foundation (Grant No. 19-41-04106).

References

1. Abali, B., Wu, C., Müller, W.: An energy-based method to determine material constants in nonlinear rheology with applications. Contin. Mech. Thermodyn. **28**(5), 1221–1246 (2016)
2. Cai, W., Moore, A., Zhu, Y., Li, X., Chen, S., Shi, L., Ruoff, R.: Thermal transport in suspended and supported monolayer graphene grown by chemical vapor deposition. Nano Lett. **10**(5), 1645–1651 (2010)
3. Calizo, I., Balandin, A., Bao, W., Miao, F., Lau, C.: Temperature dependence of the raman spectra of graphene and graphene multilayers. Nano Lett. **7**(9), 2645–2649 (2007)
4. Cao, A.: Molecular dynamics simulation study on heat transport in monolayer graphene sheet with various geometries. J. Appl. Phys. **111**(8), 083528 (2012)
5. Chen, S., Wu, Q., Mishra, C., Kang, J., Zhang, H., Cho, K., Cai, W., Balandin, A., Ruoff, R.: Thermal conductivity of isotopically modified graphene. Nat. Mater. **11**(3), 203–207 (2012)
6. Dhar, A., Kundu, A., Kundu, A.: Anomalous heat transport in one dimensional systems: a description using non-local fractional-type diffusion equation. Front. Phys. **7**, 159 (2019)
7. Dmitriev, S., Baimova, J., Savin, A., Kivshar, Y.: Ultimate strength, ripples, sound velocities, and density of phonon states of strained graphene. Comput. Mater. Sci. **53**(1), 194–203 (2012)
8. El Sachat, A., Könemann, F., Menges, F., Del Corro, E., Garrido, J., Torres, C., Alzina, F., Gotsmann, B.: Crossover from ballistic to diffusive thermal transport in suspended graphene membranes. 2D Mater. **6**(2), 025034 (2019)
9. Faugeras, C., Faugeras, B., Orlita, M., Potemski, M., Nair, R., Geim, A.: Thermal conductivity of graphene in corbino membrane geometry. ACS Nano **4**(4), 1889–1892 (2010)
10. Fehér, A., Lukács, N., Somlai, L., Fodor, T., Szücs, M., Fülöp, T., Ván, P., Kovács, R.: Size effects and beyond-fourier heat conduction in room-temperature experiments (2021). arXiv:2102.11744
11. Huberman, S., Duncan, R., Chen, K., Song, B., Chiloyan, V., Ding, Z., Maznev, A., Chen, G., Nelson, K.: Observation of second sound in graphite at temperatures above 100 k. Science **364**(6438), 375–379 (2019)
12. Hwang, G., Kwon, O.: Measuring the size dependence of thermal conductivity of suspended graphene disks using null-point scanning thermal microscopy. Nanoscale **8**(9), 5280–5290 (2016)
13. Klemens, P., Pedraza, D.: Thermal conductivity of graphite in the basal plane. Carbon **32**(4), 735–741 (1994)
14. Koukaras, E., Kalosakas, G., Galiotis, C., Papagelis, K.: Phonon properties of graphene derived from molecular dynamics simulations. Sci. Rep. **5**(1), 1–9 (2015)
15. Kovács, R., Rogolino, P.: Numerical treatment of nonlinear fourier and maxwell-cattaneo-vernotte heat transport equations. Int. J. Heat Mass Transf. **150**, 119281 (2020)
16. Kuzkin, V.: Unsteady ballistic heat transport in harmonic crystals with polyatomic unit cell. Contin. Mech. Thermodyn. **31**(6), 1573–1599 (2019)
17. Kuzkin, V., Krivtsov, A.: Fast and slow thermal processes in harmonic scalar lattices. J. Phys. Condens. Matter **29**(50), 505401 (2017)
18. Kuzkin, V., Krivtsov, A.: Ballistic resonance and thermalization in the Fermi-Pasta-Ulam-Tsingou chain at finite temperature. Phys. Rev. E **101**(4), 042209 (2020)
19. Lebon, G., Jou, D., Casas-Vázquez, J., Muschik, W.: Heat conduction at low temperature: a non-linear generalization of the guyer-krumhansl equation. Period. Polytech. Chem. Eng. **41**(2), 185–196 (1997)

20. Lepri, S., Livi, R., Politi, A.: Thermal conduction in classical low-dimensional lattices. Phys. Rep. **377**(1), 1–80 (2003)
21. Liebold, C., Müller, W.: Measuring material coefficients of higher gradient elasticity by using AFM techniques and Raman-spectroscopy. In: Generalized Continua as Models for Materials, pp. 255–271. Springer (2013)
22. Liebold, C., Müller, W.: Comparison of gradient elasticity models for the bending of micromaterials. Comput. Mater. Sci. **116**, 52–61 (2016)
23. Mak, K., Sfeir, M., Wu, Y., Lui, C.H., Misewich, J.A., Heinz, T.F.: Measurement of the optical conductivity of graphene. Phys. Rev. Lett. **101**(19), 196405 (2008)
24. Nair, R., Blake, P., Grigorenko, A., Novoselov, K., Booth, T., Stauber, T., Peres, N., Geim, A.: Fine structure constant defines visual transparency of graphene. Science **320**(5881), 1308–1308 (2008)
25. Nguyen, K., Abdula, D., Tsai, C., Shim, M.: Temperature and gate voltage dependent raman spectra of single-layer graphene. Acs Nano **5**(6), 5273–5279 (2011)
26. Northrop, G., Wolfe, J.: Ballistic phonon imaging in solids–a new look at phonon focusing. Phys. Rev. Lett. **43**(19), 1424 (1979)
27. Okamoto, N., Yanagisawa, R., Anufriev, R., A., M., Sawano, K., Kurosawa, M., Nomura, M.: Semiballistic thermal conduction in polycrystalline sige nanowires. Appl. Phys. Lett. **115**(25), 253101 (2019)
28. Saito, K., Dhar, A.: Heat conduction in a three dimensional anharmonic crystal. Phys. Rev. Lett. **104**(4), 040601 (2010)
29. Saito, R., Mizuno, M., Dresselhaus, M.: Ballistic and diffusive thermal conductivity of graphene. Phys. Rev. Appl. **9**(2), 024017 (2018)
30. Volz, S.: Microscale and Nanoscale Heat Transfer. Topics in Applied Physics, vol. 107. Springer, Berlin Heidelberg (2007)
31. Wang, L., Hu, B., Li, B., et al.: Logarithmic divergent thermal conductivity in two-dimensional nonlinear lattices. Phys. Rev. E **86**(4), 040101 (2012)
32. Xu, X., Pereira, L., Wang, Y., Wu, J., Zhang, K., Zhao, X., Bae, S., Bui, C., Xie, R., Thong, J., et al.: Length-dependent thermal conductivity in suspended single-layer graphene. Nat. Commun. **5**(1), 1–6 (2014)